# Inverse Potential Scaling in Co-Electrocatalytic Activity for CO<sub>2</sub> Reduction

## **Through Redox Mediator Tuning and Catalyst Design**

Amelia G. Reid, Juan J. Moreno, Shelby L. Hooe, Kira R. Baugh, Isobel H. Thomas, Diane A. Dickie, Charles W. Machan\*

\* - machan@virginia.edu; ORCID 0000-0002-5182-1138

AGR ORCID 0000-0002-2868-4091; JJM ORCID 0000-0003-1809-6170; SLH ORCID 0000-0002-6991-2273; DAD ORCID 0000-0003-0939-3309

Department of Chemistry, University of Virginia, PO Box 400319, Charlottesville, VA 22904-4319

### **Abstract:**

Electrocatalytic CO<sub>2</sub> reduction is an attractive strategy to mitigate the continuous rise in atmospheric CO<sub>2</sub> concentrations and generate value-added chemical products. A possible strategy to increase the activity of molecular systems for these reactions is the co-catalytic use of redox mediators (RMs), which direct reducing equivalents from the electrode surface to the active site. Recently, we demonstrated that a sulfone-based RM could trigger co-electrocatalytic CO<sub>2</sub> reduction via an inner-sphere mechanism under aprotic conditions. Here, we provide support for inner-sphere cooperativity under protic conditions by synthetically modulating the mediator to increase activity at lower overpotentials (inverse potential scaling). Furthermore, we show that both the intrinsic and co-catalytic performance of the Cr-centered catalyst can be enhanced by ligand design. By tuning both the Cr-centered catalyst and RM appropriately, an optimized coelectrocatalytic system with quantitative selectivity for CO at an overpotential (η) of 280 mV and turnover frequency (TOF) of 194 s<sup>-1</sup> is obtained, representing a two-fold increase in co-catalytic activity over our original report at 130 mV lower overpotential. Importantly this work lays the foundation of a powerful tool for developing catalytic systems for CO<sub>2</sub> reduction.

#### **Introduction:**

The interest in electrochemical carbon dioxide (CO<sub>2</sub>) reduction is two-fold: the association of climate change with the global rise in atmospheric CO<sub>2</sub> concentrations and the increasing need to transition from non-renewable fossil fuel-derived hydrocarbons as chemical feedstocks and energy sources.<sup>1</sup> The reduction of CO<sub>2</sub> to CO could help to mitigate both of these issues through conversion of CO<sub>2</sub> into useful building blocks for the synthesis of chemical feedstocks and fuels while using renewable energy sources, such as sunlight and wind, as the source of electricity.<sup>2</sup> In recent years, the focus of molecular electrocatalyst development has shifted towards the use of abundant first-row transition metal centers to address the need for cost-effective and scalable systems.<sup>4-8</sup>

Nature frequently leverages co-catalytic systems during reactions involving electron transfer. For example, during cellular respiration the electron transport chain uses several redox mediators (RMs) to shuttle protons and electrons between different redox-active cofactors. The final step of this cycle involves ubiquinone shuttling electrons and protons to cytochrome *c* oxidase as a part of the overall reduction of dioxygen to water. Co-catalytic systems which utilize RMs have been successfully developed for homogeneous O<sub>2</sub> reduction, increasing the overall activity of the system and shifting the selectivity of the reaction. Parallel developments have enabled electrocatalytic N<sub>2</sub> reduction, where weak C–H bonds are generated in a metallocene-based RM to assist in the cleavage of inert bonds, and alcohol oxidation, where RMs are utilized to facilitate hydrogen atom transfer processes that work in conjunction with the catalyst. Additional work has focused on the use of small-molecule RMs for the CO<sub>2</sub> reduction reaction on heterogeneous surfaces. Smith *et al.* reported the first homogeneous co-electrocatalytic system for the reduction of CO<sub>2</sub> using a NADH analogue as the RM and an Fe tetraarylporphyrin complex that shows

enhanced catalytic activity as a combined system.<sup>17</sup> The NADH analogue transfers protons and electrons during the reaction, although the exact reaction sequence is currently unknown.

Recently, we reported a co-electrocatalytic system comprised of a chromium-centered catalyst, Cr(tbudhbpy)Cl(H2O) (1),8,18 and dibenzothiophene 5,5-dioxide (DBTD) as the RM.19 When both species are present under aprotic conditions, the co-catalytic reductive disproportionation of two equivalents of CO<sub>2</sub> occurs to produce CO and CO<sub>3</sub><sup>2-</sup>. Because neither the catalyst nor the mediator demonstrates intrinsic reactivity for CO<sub>2</sub> reduction, an outer-sphere mechanism could be excluded. For clarity, the following labeling scheme will be used for Cr complexes # bound DMF Cr(axial ligands) charge and for RM species multiplicity RM charge; the ligand frameworks do not change the  $\kappa^4$  coordination mode during the reaction, so it is omitted in the notation where possible for clarity. These studies suggested that that the assembly of  $^{2}$  **DBTD**<sup>-1</sup> with an intermediate bis-CO<sub>2</sub> adduct,  $^{4}_{0}$ Cr(CO<sub>2</sub>CO<sub>2</sub>)<sup>-1</sup>, through inner-sphere coordination produces a dianion,  ${}_{0}^{3}$   $Cr(CO_{2}CO_{2})(DBTD)^{-2}$ , which mediates carbon-oxygen bond cleavage. Association between the catalyst and mediator monoanions under aprotic conditions is driven by contributions from dispersive interactions, Cr-O bond formation between the metal complex and [DBTD], and through-space electronic conjugation (TSEC, Figure 1) between the ligand backbone of the catalyst and the RM. TSEC is a non-covalent interaction between cofacial aromatic rings based on the interaction of their spatially delocalized  $\pi$  electrons.<sup>20</sup>

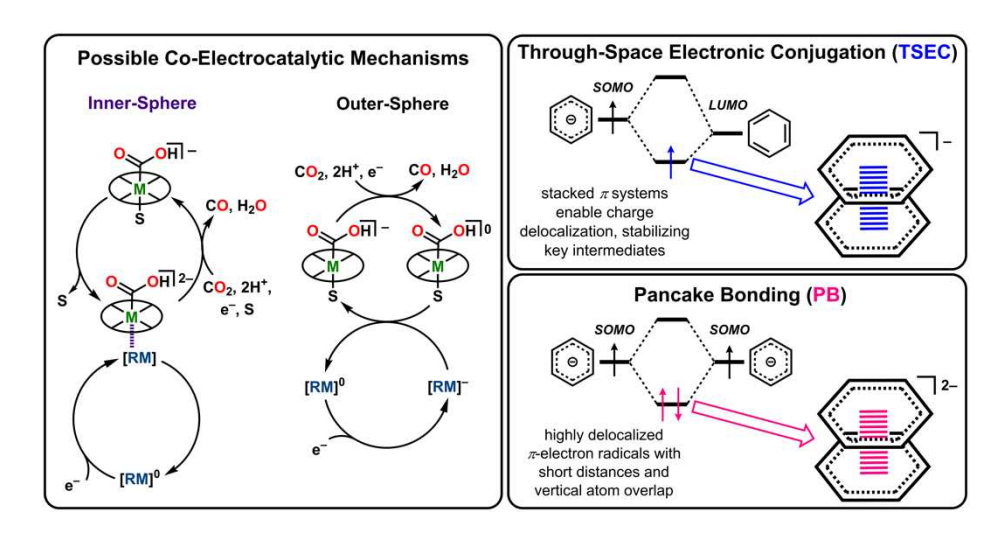


**Figure 1.** Overview of protic CO<sub>2</sub> reduction co-electrocatalysis, through-space electronic conjugation, and pancake bonding interactions relevant to the results presented here.

When phenol (PhOH) is added as a sacrificial proton source under co-catalytic conditions there is an increase in activity compared to when only 1 or DBTD is present. 8, 19 It was proposed that the association under protic conditions is driven in part by pancake bonding (PB, Figure 1), which is a parallel  $\pi$ -stacking interaction between planar aromatic moieties with significant radical character.<sup>21-24</sup> Under co-electrocatalytic conditions, PB favors an equilibrium solvent displacement from  ${}_{1}^{3}\text{Cr(CO}_{2}\text{H})^{-1}$  by  ${}^{2}\text{DBTD}^{-1}$  to form the dianion  ${}_{0}^{4}\text{Cr(CO}_{2}\text{H})(\text{DBTD})^{-2}$ , with contributions from chromium-sulfone coordination and dispersive interactions. In this bimolecular assembly under protic conditions, both the [RM] and the bipyridine (bpy) fragment of the [Cr-CO<sub>2</sub>H]<sup>-</sup> complex are formally reduced by one electron, consistent with PB. However, since the Cr catalyst itself has intrinsic CO<sub>2</sub> reduction activity when PhOH is present, we could not definitively discard the possibility that [DBTD] enhanced reactivity by outer-sphere electron transfer (Figure 1). We reasoned that the strength of the interaction between the RM and Cr complex could be increased by synthetic means, since it has been noted that the strength of PB generally scales with respect to the extent of  $\pi$ -electron delocalization in the participating radicals and their steric protection from sigma-bonding interactions.<sup>24</sup>

Here, we compare the activity and overpotential  $(\eta)$  of two Cr catalysts with four RM architectures, to better understand and optimize the co-electrocatalytic system under protic conditions. These results suggest that extended aromatic character in the RM structure has the dual benefit of lowering its standard reduction potential while also favoring its binding to the Cr complex, resulting in inverse reaction scaling where increased activity occurs at lower overpotentials. We propose that mediator designs which extend aromatic character and match redox potential with the metal complex induce stronger interactions that improve the stability and activity of co-electrocatalysis, without requiring changes in the coordinating strength of the axial sulfone ligand.

### **Results:**

### **Electrochemistry of Cr Catalysts**

The synthesis of the 6,6'-di(3,5-di-*tert*-butyl-2-hydroxybenzene)-2,2'-bipyridine ('budhbpy(H)<sub>2</sub>) ligand and its subsequent metalation to generate Cr('budhbpy)Cl(H<sub>2</sub>O) (1) was carried out as previously reported (**Figure S1**). To improve the catalyst activity we synthesized a ligand framework with electron-donating *tert*-butyl groups on the bpy-backbone, 6,6'-di(3,5-di-*tert*-butyl-2-hydroxybenzene)-4,4'-di-*tert*-butyl-2,2'-bipyridine ('budhtbubpy(H)<sub>2</sub>) which allows us to probe ligand electronic effects on the catalyst and co-catalytic system (see Supporting Information (SI) and **Figures S2-S4**). The metalation of ('budhtbubpy(H)<sub>2</sub>) to form Cr('budhtbubpy)Cl(H<sub>2</sub>O) (2) was carried out in a similar fashion to 1 (SI) and 2 was characterized by UV-vis (**Figure S5**), NMR (**Table S3**), electrospray ionization-mass spectrometry (ESI-MS) (SI), microanalysis (SI), and single-crystal X-ray diffraction (XRD) studies (**Figure 2**).

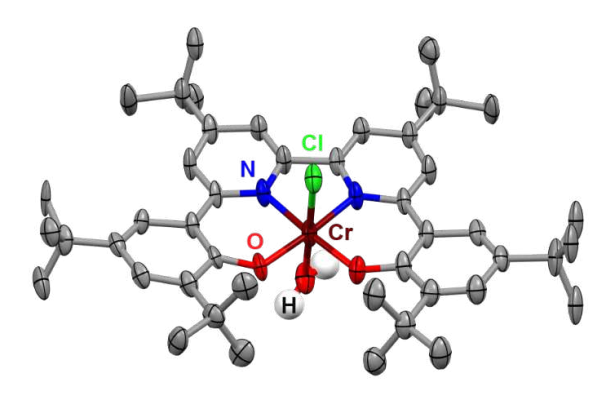


**Figure 2.** Molecular structure of Cr(<sup>tbu</sup>dh<sup>tbu</sup>bpy)Cl(H<sub>2</sub>O) (**2**) obtained from single-crystal X-ray diffraction studies. Blue = N, red = O, gray = C, green = Cl, maroon = Cr, white = H atoms of bound water molecule; thermal ellipsoids at 50%; ligand H atoms and occluded diethyl ether molecules omitted for clarity; hydrogen atoms of the Cr-bound water molecule were located in the diffraction map and refined isotropically. CCDC 2150930.

Cyclic voltammetry (CV) experiments were performed on 1 and 2 in N,N-dimethylformamide (DMF) with 0.1 M tetrabutylammonium hexafluorophosphate (TBAPF<sub>6</sub>) as the supporting electrolyte. As reported previously, 1 exhibits three redox features under argon (Ar) saturation conditions,  $E_p = -1.66$  and -1.78 V and  $E_{1/2} = -1.95$  V versus the ferrocenium/ferrocene (Fc<sup>+</sup>/Fc) reduction potential. Complex 2 also exhibits three redox features, but due to the electron-donating quality of the *tert*-butyl groups on the bpy core of the ligand, all three are located at the more negative potentials of  $E_p = -1.76$  and -1.87 V and  $E_{1/2} = -2.00$  V vs. Fc<sup>+</sup>/Fc (Figure S6). The first two redox features of 1 were shown to be related to one another, previously assigned to the formation of a solvento species resulting from an equilibrium chloride displacement reaction. Due to the consistencies in redox potential, reversibility, and relative current intensities of these features in 2, the same can be concluded here. As was the case with 1, the first two reduction features coalesce at scan rates  $\geq 2000$  mV/s, which is consistent with this assignment (Figure S7).

Upon the addition of PhOH under Ar saturation conditions, 1 and 2 demonstrate only a small change in the redox features, suggestive of either hydrogen bonding interactions between

the reduced complex and PhOH or increased favorability of chloride anion solvation, but not formal protonation.<sup>25-27</sup> Under CO<sub>2</sub> saturation without PhOH, there are minimal changes to the redox features for both catalysts, meaning that aprotic CO<sub>2</sub> reduction is not inherent to either 1 or 2. Variable scan rate analysis under both Ar and CO<sub>2</sub> saturation shows that the electron transfer reaction is diffusion-controlled for 2 at the third reduction feature, indicating a homogenous electrochemical response (**Figures S7** and **S8**) as was observed previously for 1.<sup>8</sup>

The similarity of the redox activity between complexes 1 and 2 extends to catalytic behavior: 2 also catalyzes  $CO_2$  reduction at the third redox feature ( $E_{cat/2} = -2.00 \text{ V}$  vs.  $Fc^+/Fc$ ) in the presence of PhOH. However, 2 more than doubles the amount of current density (1.38 mA/cm², **Figure 3B**, red) under the same conditions as 1 (0.554 mA/cm², **Figure 3B**, black). This significant increase in current density comes with a shift of only 50 mV to more negative potentials, increasing the  $\eta$  from 110 mV to 160 mV (see **SI**). Complex 1 was previously found to have first-order concentration dependences with respect to electrocatalytic current for PhOH, catalyst, and  $CO_2$ .8 Performing the same variable concentration experiments with 2 (**Figures S9-S11**) established that this system also has first-order concentration dependences with respect to PhOH (**Figures S9**), catalyst (**Figure S10**), and  $CO_2$  (**Figure S11**) on electrocatalytic current.

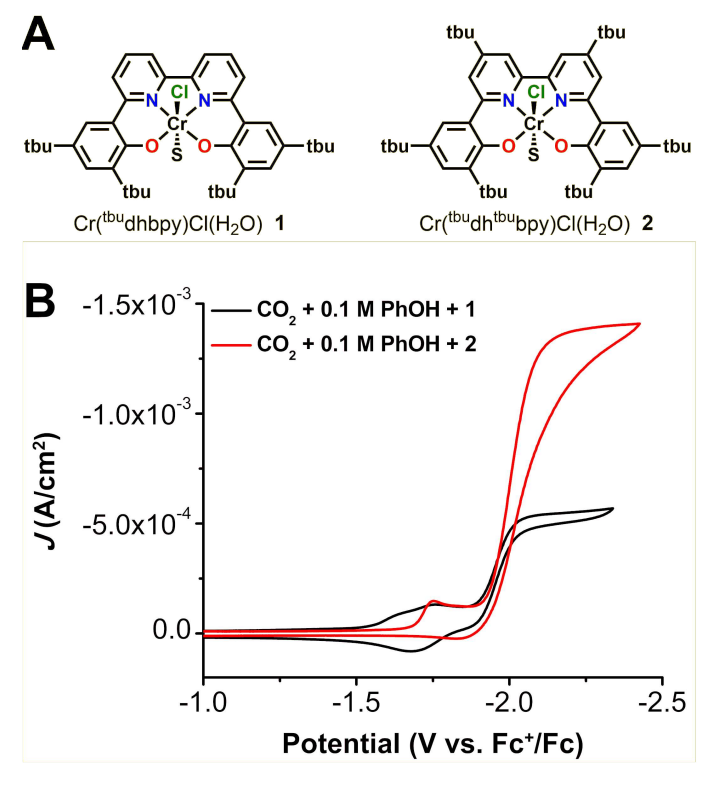


**Figure 3.** (**A**) Structures of Cr(tbudhbpy)Cl(H<sub>2</sub>O) **1** and Cr(tbudhtbubpy)Cl(H<sub>2</sub>O) **2**, where S is a solvent adduct of water or DMF. (**B**) Comparison of CVs for different Cr catalysts (1.0 mM) under CO<sub>2</sub> saturation conditions and 0.1 M PhOH. Conditions: 0.1 M TBAPF<sub>6</sub>/DMF; glassy carbon working electrode, glassy carbon rod counter electrode, Ag/AgCl pseudoreference electrode; referenced to Fc<sup>+</sup>/Fc internal standard; 100 mV/s scan rate.

To quantify the product selectivity and turnover frequency (TOF) of  $\mathbf{2}$ , controlled potential electrolysis (CPE) was performed with added PhOH under CO<sub>2</sub> saturation conditions (**Figure S12**). Gaseous products were quantified by gas chromatography (GC, see **SI**). The results of this experiment (**Table S4**) show that  $\mathbf{2}$  is selectively reducing CO<sub>2</sub> to CO under these conditions with  $95 \pm 8\%$  FE<sub>CO</sub> over 13.0 turnovers (turnover represents two electron equivalents of charge passed for each equivalent of  $\mathbf{2}$  in solution) with a TOF<sub>CPE</sub> of  $9.29 \text{ s}^{-1}$  which is in good agreement with the TOF<sub>max</sub> value of  $14\pm1 \text{ s}^{-1}$  determined by CV (**Figures S13-14** and **Table S5**). Note that in all instances turnovers have been determined to show the catalytic nature of the process and *do not represent a measurement to complete loss of activity*.

## **Electrochemistry of Redox Mediators**

To test the inner-sphere nature of the co-electrocatalytic mechanism we previously reported and further optimize the system, <sup>19</sup> we prepared three new aromatic sulfone derivatives to establish structure-activity relationships with Cr catalysts 1 and 2. Triphenylothiophene-4,4-dioxide (TPTD, Figure 4A) was synthesized by previously reported methods.<sup>29, 30</sup> Additionally, both 2,8dimesityldibenzothiophene-5,5-dioxide (Mes<sub>2</sub>DBTD) and 2,8-diphenyldibenzothiophene-5,5dioxide (Ph<sub>2</sub>DBTD) (Figure 4A) were prepared using Pd-catalyzed cross-coupling and characterized by NMR (Figures S15-S18), ESI-MS (SI), microanalysis (SI), and XRD studies (Figure 4A). CV experiments were carried out under the same conditions as 1 and 2, in 0.1 M TBAPF<sub>6</sub> with DMF as the solvent. Under Ar saturation conditions, DBTD displays a reversible redox feature with an  $E_{1/2} = -2.25$  V versus Fc<sup>+</sup>/Fc corresponding to a single-electron event.<sup>19</sup> TPTD, Mes<sub>2</sub>DBTD, and Ph<sub>2</sub>DBTD also show single reversible one-electron redox features under Ar saturation conditions, but the  $E_{1/2}$  values for all three are shifted to more positive potentials compared to DBTD (Figure 4B). Mes<sub>2</sub>DBTD has the most similar redox feature to DBTD with an  $E_{1/2} = -2.24$  V versus Fc<sup>+</sup>/Fc, while TPTD and Ph<sub>2</sub>DBTD shift to more positive potentials with  $E_{1/2} = -2.19 \text{ V}$  and -2.12 V versus Fc<sup>+</sup>/Fc, respectively.

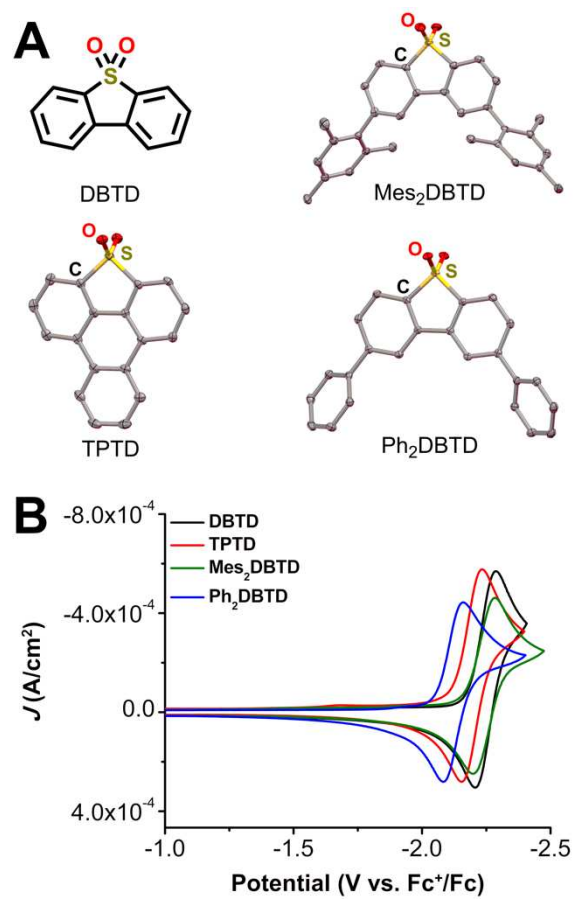


**Figure 4.** (**A**) Structures of redox mediators dibenzothiophene-5,5-dioxide (DBTD), triphenylothiophene-4,4-dioxide (TPTD), 2,8-dimesityldibenzothiophene-5,5-dioxide (Mes<sub>2</sub>DBTD), and 2,8-diphenyldibenzothiophene-5,5-dioxide (Ph<sub>2</sub>DBTD). TPTD, Mes<sub>2</sub>DBTD, and Ph<sub>2</sub>DBTD obtained from single-crystal X-ray diffraction studies. Yellow = S, red = O, gray = C; thermal ellipsoids at 50%; H atoms and occluded toluene molecules (Ph<sub>2</sub>DBTD only) omitted for clarity. CCDC 215497-215499. (**B**) Comparison of CVs for different RMs (2.5 mM) under Ar saturation. Conditions: 0.1 M TBAPF<sub>6</sub>/DMF; glassy carbon working electrode, glassy carbon rod counter electrode, Ag/AgCl pseudoreference electrode; referenced to Fc<sup>+</sup>/Fc internal standard; 100 mV/s scan rate.

Control experiments performed with TPTD, Mes<sub>2</sub>DBTD, and Ph<sub>2</sub>DBTD demonstrate little reactivity with CO<sub>2</sub> or PhOH on the CV timescale, as was previously observed for analogous experiments with DBTD (**Figures S19-S21**). Variable scan rate experiments were performed for all four sulfone derivatives to calculate their diffusion coefficients (**Figures S22-S25**, see **SI**).<sup>31</sup> Unsurprisingly, the experimentally determined diffusion coefficients for these molecules scale

with their molecular weight: DBTD (6.22 x  $10^{-6}$  cm<sup>2</sup>/s) > TPTD (3.93 x  $10^{-6}$  cm<sup>2</sup>/s) > Ph<sub>2</sub>DBTD (3.68 x  $10^{-6}$  cm<sup>2</sup>/s) > Mes<sub>2</sub>DBTD (3.57 x  $10^{-6}$  cm<sup>2</sup>/s).

## **Co-Electrocatalysis Under Protic Conditions**

Since the addition of PhOH as a sacrificial proton donor led to a large increase in catalytic activity for 1+DBTD in previous studies, we sought to see if a similar trend would be observed for 1 with the new RMs and 2 with all four RMs. Briefly, the observed trend in current density under CV conditions for all the RMs when added to a solution of 1 and PhOH can be summarized: DBTD has the highest increase in current followed by TPTD, and Ph<sub>2</sub>DBTD shows a slightly greater current increase than Mes<sub>2</sub>DBTD *despite having a standard potential which is 120 mV more positive in its one-electron reduction potential* (Figure 5A). However, the addition of all four RMs exhibit a significant increase in current and completely irreversible waveforms. Variable concentration studies were completed for 1, all four RMs, PhOH, and CO<sub>2</sub>. These data show that the observed current is proportional to the concentration of 1 (Figures S29-S31), RM (Figure S32-S34), a fixed ratio of 1 and RM (Figure S35-S37), PhOH (Figure S38-S40), and CO<sub>2</sub> (Figure S41-S43) where RM is DBTD, <sup>19</sup> TPTD, Mes<sub>2</sub>DBTD, and Ph<sub>2</sub>DBTD.

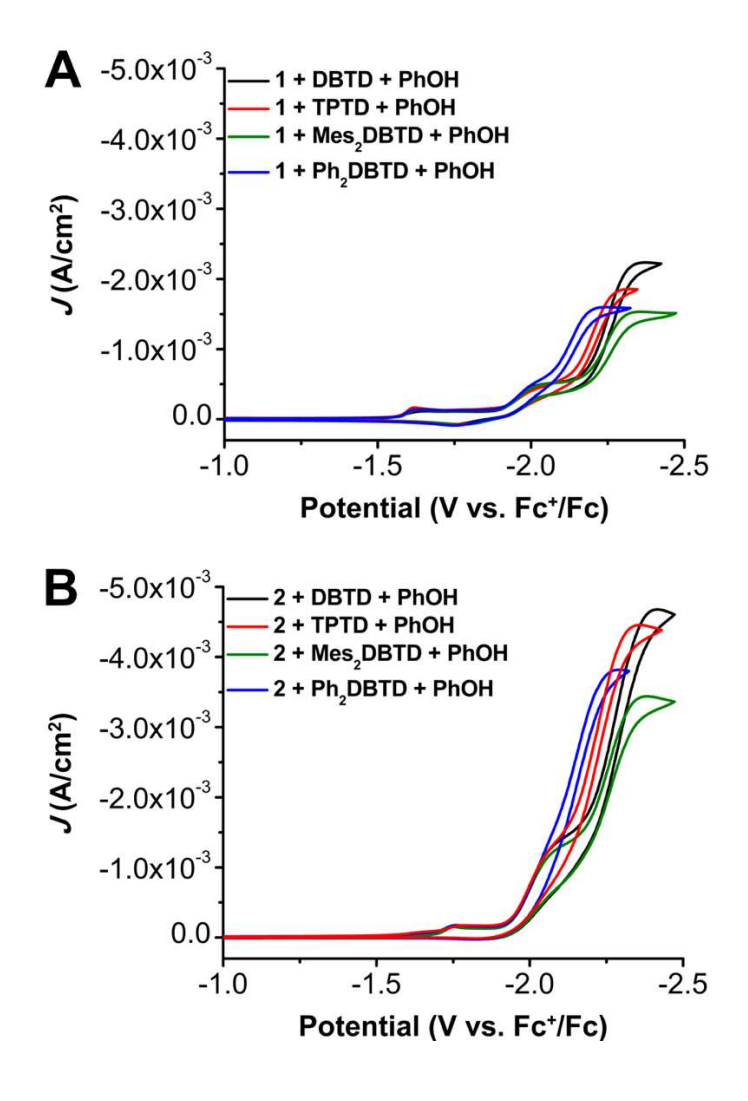


**Figure 5.** CVs of 1.0 mM Cr(<sup>tbu</sup>dhbpy)Cl(H<sub>2</sub>O) **1** (**A**) or Cr(<sup>tbu</sup>dh<sup>tbu</sup>bpy)Cl(H<sub>2</sub>O) **2** (**B**) with 2.5 mM DBTD (black), TPTD (red), Mes<sub>2</sub>DBTD (green), and Ph<sub>2</sub>DBTD (blue) as the RM and 0.1 M PhOH under CO<sub>2</sub> saturation conditions. Conditions: 0.1 M TBAPF<sub>6</sub>/DMF; glassy carbon working electrode, glassy carbon rod counter electrode, Ag/AgCl pseudoreference electrode; referenced to Fc<sup>+</sup>/Fc internal standard; 100 mV/s scan rate.

When we compare the protic catalytic activity of **2** with all the RMs, we see a similar trend to the activity of **1** observed under comparable conditions. DBTD again shows the greatest increase in current followed by TPTD under CV conditions (**Figure 5B**). However, for complex **2** there is a significant difference in the activity of the co-catalytic system with Ph<sub>2</sub>DBTD relative to that with Mes<sub>2</sub>DBTD; Ph<sub>2</sub>DBTD again outperforms Mes<sub>2</sub>DBTD as a RM when paired with **2** despite

its more positive standard reduction potential. Since 2 is an intrinsically better catalyst than 1 under CO<sub>2</sub> saturation with a proton donor, we were delighted to find that co-electrocatalysis involving 2 and the four RMs under protic conditions also reached much larger current densities than any combination involving 1. Variable concentration experiments were also performed for 2, all four RMs, a fixed ratio of complex 2 and all RMs, PhOH, and CO<sub>2</sub>, demonstrating proportional increases in current with respect to each reaction component (see Figures S48-S67).

CPE experiments were performed in the presence of 0.12 M PhOH with 1 or 2 and across three concentrations of DBTD, TPTD, Mes<sub>2</sub>DBTD, and Ph<sub>2</sub>DBTD (Figures S68-S74). The current observed during the CPE experiments with 1 as the catalyst scaled with increasing RM concentration at the tested catalyst:RM ratios of 1:1, 1:3, and 1:5 (Ref<sup>19</sup> and Figures S68-S70). However, this did not hold true for all RM combinations with 2. When TPTD, Mes<sub>2</sub>DBTD, and Ph<sub>2</sub>DBTD were used as the RM, the observed current scaled with respect to their concentration. However, when DBTD was used as the RM with 2, saturation was observed at the 1:3 ratio with no further increase observed at the 1:5 ratio (Figure S71). Both catalysts with all mediators at all ratios tested were found to be quantitatively selective for CO (Tables S7-S27). However, since the 1:5 (catalyst:RM) produced the largest amount of CO on average for all the systems, we will focus the remainder of our analysis on these experiments. All combinations of the protic coelectrocatalytic systems show high activity with TOF values ranging from 64.0 to 208 s<sup>-1</sup> (**Table** 1), one to two orders of magnitude higher than the catalysts alone. As was the case for DBTD, 19 control CPE experiments for TPTD, Mes<sub>2</sub>DBTD, and Ph<sub>2</sub>DBTD in the presence of PhOH without catalyst (Figures S75-S77) show non-quantifiable amounts of CO (Tables S28-S30). Additionally, to understand the stability of DBTD during electrolysis, a control CPE of DBTD and PhOH under N<sub>2</sub> was performed (Figure S78). Characterization of the pre- and post-CPE solution by gas chromatography/mass spectrometry (GC/MS) with appropriate controls demonstrates minor amounts of DBTD is reduced to the corresponding sulfoxide, dibenzothiophene 5-oxide (DBTO; **Figure S78**). However, while comparable analysis of the CPE solution before and after the experiment under catalytic conditions (1, DBTD, and PhOH under CO<sub>2</sub>) also shows reduction of DBTD to DBTO, an additional product with a mass too high to be dibenzothiophene is detected, implying that reductive C–S bond cleavage is a possible degradation pathway (**Figure S79**). It is worth emphasizing that the high catalytic efficiencies observed under all measured conditions suggest that these pathways are minor contributors for all systems (**Table 1**).

Table 1. Results of CPE experiments with PhOH under CO<sub>2</sub> saturation conditions.

Conditions	Potential	FE <sub>CO</sub> (%)	TOF <sub>CPE</sub> s <sup>-1</sup>	η (V)	Turnovers	Turnovers	$i_{\rm cat}/i_{ m p}$
	(V vs				of CO	of CO	
	Fc <sup>+</sup> /Fc)				w.r.t [1 or 2]	w.r.t [RM]	
<b>1</b> + PhOH <sup>19, a</sup>	-2.30	111±14	7.12	0.11	11.4	_	3.4
1 + DBTD + PhOH <sup>19, b</sup>	-2.30	102±14	65.3	0.41	29	5.8	2.8
1 + TPTD + PhOH <sup>c</sup>	-2.25	98±17	74.5	0.35	25	4.9	3.0
1 + Mes <sub>2</sub> DBTD + PhOH <sup>c</sup>	-2.30	98±6	64.0	0.40	19	4.7	2.6
1 + Ph <sub>2</sub> DBTD + PhOH <sup>c</sup>	-2.20	100±2	69.3	0.28	22	5.3	3.6
$2 + PhOH^d$	-2.30	95±8	9.29	0.16	13	_	8.4
2 + DBTD + PhOH <sup>c</sup>	-2.30	109±9	163	0.41	28	6.5	5.8
2 + TPTD + PhOH <sup>c</sup>	-2.25	97±6	208	0.35	31	8.0	6.6
2 + Mes <sub>2</sub> DBTD + PhOH <sup>c</sup>	-2.30	98±4	149	0.40	27	5.9	5.7
2 + Ph <sub>2</sub> DBTD + PhOH <sup>c</sup>	-2.20	97±5	194	0.28	35	8.8	7.1

<sup>&</sup>lt;sup>a</sup> – 0.5 mM catalyst and 0.6 M PhOH

<sup>&</sup>lt;sup>b</sup> – 0.5 mM catalyst, 2.5 mM RM, and 0.6 M PhOH

<sup>&</sup>lt;sup>c</sup> – 0.1 mM catalyst, 0.5 mM RM, and 0.12 M PhOH

<sup>&</sup>lt;sup>d</sup> – 0.1 mM catalyst and 0.12 M PhOH

The systems with 1 and 2 as the catalyst followed the same trend in TOF<sub>CPE</sub> for CO formation when comparing across the RMs: Mes<sub>2</sub>DBTD < DBTD < Ph<sub>2</sub>DBTD < TPTD (**Table** 1). As introduced above, our proposed inner-sphere mechanism for this co-electrocatalytic reaction relies on the binding of the reduced RM to an intermediate [Cr-CO<sub>2</sub>H]<sup>-</sup> species before the ratedetermining C-OH bond cleavage step. 19 Although all RMs are reducing enough to transfer electron equivalents via an outer-sphere mechanism, the data presented in Table 1 are most consistent with the predominance of an inner-sphere RM pathway: the observed co-catalytic activity does not scale with the reduction potential of the RMs or their diffusion coefficients. For a purely outer-sphere mechanism, conformity to a Marcus theory-type model would be expected, where increased electrochemical driving force would equate to an increased rate of reaction (under the assumption that the inverted region or diffusion limit are not reached under experimental conditions).<sup>32</sup> Instead, the two RMs with the most positive standard reduction potentials (TPTD and Ph<sub>2</sub>DBTD) demonstrate the greatest activity. Likewise, if outer-sphere electron transfer was the primary reaction pathway, the relatively slowly diffusing Ph<sub>2</sub>DBTD would be expected to show decreased activity compared to DBTD, however an opposite trend is observed experimentally. The relatively limited performance of the Mes<sub>2</sub>DBTD derivative despite a similar reduction potential to DBTD suggests that sterically encumbering the dibenzothiophene-5,5-dioxide core has a kinetic effect, which is also consistent with an inner-sphere pathway causing the greatest activity enhancement. The optimized combination of 2+Ph<sub>2</sub>DBTD under protic conditions achieves a TOF of 194 s<sup>-1</sup> at an η of 280 mV, which demonstrates a three-fold increase in activity at an η which is 130 mV less in comparison to the previous system with 1 and DBTD.<sup>19</sup>

The trend in activity data derived from CPE is at first glance different than the overall current trend observed in the CV data (Figure 5). However, homogeneous current density is

dependent on the diffusion coefficients of reaction components under experimental conditions. In an effort to account for this difference and the effect it has on the observed trend in the CV data, we have calculated the value of  $i_{cat}/i_p$  ( $i_{cat}$  = catalytic plateau current and  $i_p$  = Faradaic current) for each of the co-catalytic systems at the redox feature of the respective mediators. Under appropriate conditions, this experimental value can be used to calculate a TOF<sub>max</sub> value from CV data and represents relative catalytic activity when compared across systems (**Table 1** and **Figure S80**; see the SI for details).<sup>33</sup> The trend observed for the  $i_{cat}/i_p$  ratios is generally consistent with the TOF<sub>CPE</sub>: the co-catalytic Ph<sub>2</sub>DBTD and TPTD systems have larger activities than the other RMs. It should be emphasized that since RM and Cr complexes do not interact under Faradaic conditions, we are unable to use this method to calculate TOF<sub>max</sub> values, although we note that the relative trend of the current ratios still qualitatively describes differences in activity observed in CPE experiments.

### **Computational Studies**

To gain insight into the assembly of RMs and catalysts, DFT calculations were done with the Gaussian 16 package at the B3LYP-D3(BJ)/def2-tzvp//B3LYP-D3(BJ)/def2-svp level of theory (see SI for details). As previously reported, including dispersion corrections at the optimization stage is of paramount importance due to the key role of non-covalent interactions. The free energies of formation of the dianionic  ${}^{4}_{0}$ Cr(CO<sub>2</sub>H)(RM) $^{-2}$  assemblies for 1 and 2 summarized by Eq (1) are collected in Table 2.

$${}_{1}^{3}\text{Cr(CO}_{2}\text{H)}^{-1} + {}^{2}\text{RM}^{-1} \rightleftharpoons {}_{0}^{4}\text{Cr(CO}_{2}\text{H)(RM)}^{-2} + \text{DMF}$$
 Eq (1)

Table 2. Calculated free energies of [RM] ligand displacement reaction summarized by Eq (1), calculated free energies of activation for the rate-limiting C-OH bond cleavage step and

experimental redox potentials of the RMs vs  $Fc^+/Fc$ . S = DMF.

Cr Complex	RM	$\Delta G \operatorname{Eq} (1)$	$\Delta G^{\ddagger}$ C-OH	RM <sup>0/-</sup> vs
_		(kcal/mol)	(kcal/mol)	$Fc^{+/0}$
[Cr(tbudhbpy)(CO <sub>2</sub> H)S)]	none	n/a	13.5	n/a
[Cr(tbudhbpy)(CO <sub>2</sub> H)S)] <sup>-</sup>	[DBTD] <sup>-</sup>	-0.1	11.6	-2.25
[Cr(tbudhbpy)(CO <sub>2</sub> H)S)] <sup>-</sup>	$[Mes_2DBTD]^-$	0.5	-	-2.24
[Cr(tbudhbpy)(CO <sub>2</sub> H)S)]	$[TPTD]^-$	-2.9	11.6	-2.19
[Cr(tbudhbpy)(CO <sub>2</sub> H)S)] <sup>-</sup>	$[Ph_2DBTD]^-$	-3.1	11.6	-2.12
[Cr(tbudhtbubpy)(CO <sub>2</sub> H)S)]	none	n/a	12.5	n/a
[Cr(tbudhtbubpy)(CO <sub>2</sub> H)S)]	[DBTD] <sup>-</sup>	-2.3	10.7	-2.25
[Cr(tbudhtbubpy)(CO <sub>2</sub> H)S)]	[Mes <sub>2</sub> DBTD] <sup>-</sup>	-2.0	-	-2.24
$[Cr(^{tbu}dh^{tbu}bpy)(CO_2H)S)]^-$	$[TPTD]^-$	-6.6	10.9	-2.19
[Cr(tbudhtbubpy)(CO <sub>2</sub> H)S)]	[Ph <sub>2</sub> DBTD] <sup>-</sup>	-6.1	10.8	-2.12

Despite Coulombic repulsion, the substitution of a DMF molecule for the reduced mediator is favorable in almost all cases, reaching large free energies of reaction of -6.1 and -6.6 kcal/mol for the combination of Ph<sub>2</sub>DBTD and TPTD with **2**. These values show good correlation with the experimental TOF values for **2**, while for **1** the trend is less pronounced (**Figure 6**). Indeed, while transition state energies determined for the dianionic assemblies of DBTD, TPTD, and Ph<sub>2</sub>DBTD RMs with both complexes **1** and **2** show minimal variance with respect one another (**Table 2**), they are uniformly lower than the comparable transition state energy of the monoanionic DMF adduct. In other words, the solvento species for both complexes **1** and **2** lies on a higher-energy pathway than any of the co-catalytic combinations studied. Importantly, this result implies that the equilibrium represented in **Eq (1)** has a direct effect on catalyst speciation relevant to the observed activity.

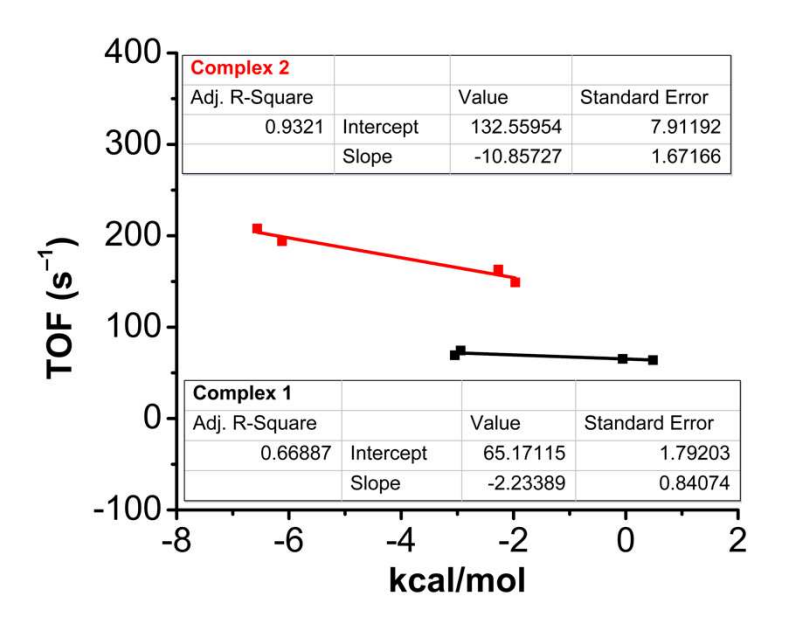
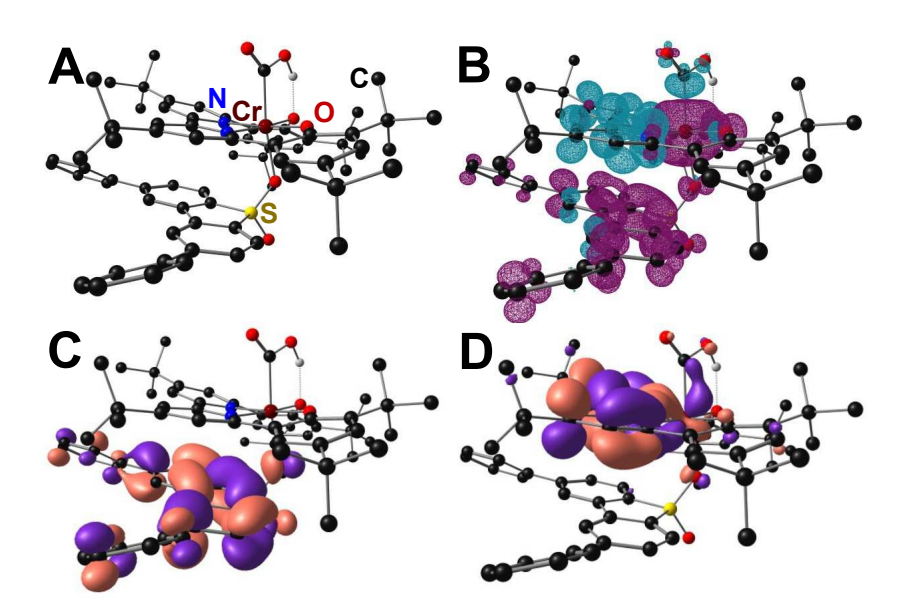


Figure 6. Correlation between computed DMF displacement energies and TOF.

The apparent PB interaction can be visualized in the spin density plots and Kohn-Sham orbital representations occupied molecular orbitals of of the singly the  ${}^4_0\text{Cr}(\text{CO}_2\text{H})(\text{Ph}_2\text{DBTD})^{-2}$  adduct (Figure 7). In addition to the favorable energetics of the association of the Ph<sub>2</sub>DBTD and the Cr complex, these plots show antiferromagnetic coupling between Ph<sub>2</sub>DBTD and the bpy fragment of the ligand in singly occupied orbitals of relevant symmetries. While a PB between [RM]<sup>-</sup> and [Cr-CO<sub>2</sub>H]<sup>-</sup> requires sufficient extended aromatic character, another component of fundamental importance for any bonding interaction is that in order to be maximized, orbitals need to be close both in terms of orbital shape and energy. In other words, we propose that the PB is maximized as the standard potential of the RM approaches that of the catalyst because the radical-containing orbitals of the reduced aromatic fragments become closer in energy. NICS(0) calculations on all RMs in the neutral and radical anion states indicate that the five-membered sulfone-containing ring goes from antiaromatic to aromatic upon reduction (**Tables S31-S34**). KS representations of all  ${}_0^4$ Cr(CO<sub>2</sub>H)(RM) $^{-2}$  adducts show that orbitals from this five-membered ring are key to the proposed PB, interacting with the partially occupied  $\pi^*$  orbitals of the bpy fragment in the Cr complex relevant to the co-catalytic pathway. 18, 19

It is worth stating again, however, that with the present data the observed correlation is weak for complex 1. This suggests that while RM redox potentials are to some extent an indirect measure of relevant orbital energies, there are additional kinetic components influenced by the steric bulk of the catalyst and the RM. This kinetic effect is seen most directly in the comparison of the experimental and computational data of DBTD and Mes<sub>2</sub>DBTD, which despite being nearly identical in terms of redox potential have significantly different activity and calculated association energies.



**Figure 7**. Molecular geometry of the  ${}_{0}^{4}$ Cr(CO<sub>2</sub>H)(Ph<sub>2</sub>DBTD) $^{-2}$  adduct (A) DFT-calculated spin density (B) Kohn-Sham orbital projection of SOMO (C) and SOMO $^{-1}$  (D).

## Analysis of Electrochemical CO<sub>2</sub> Reduction Under Aprotic Conditions

Previously we observed that the addition of DBTD to a solution of 1 under CO<sub>2</sub> saturation conditions lead to the appearance of an aprotic catalytic feature that is not intrinsic to either

component.<sup>19</sup> The addition of TPTD (**Figure S86**) to a solution of **1** and CO<sub>2</sub> leads to the appearance of an irreversible redox feature at the  $E_{1/2}$  of TPTD (-2.19 V vs. Fc<sup>+</sup>/Fc), although the increase is less than that observed for DBTD. Despite a 120 mV difference in standard potential, Mes<sub>2</sub>DBTD and Ph<sub>2</sub>DBTD RMs demonstrate roughly the same increase in the observed current density and some retention of the return oxidation feature of the RM. This suggests an excess of the RM radical anion is being generated with respect to its rate of interaction with complex **1**, and as a result, on the return CV sweep the radical anion is still present for re-oxidation, leading to the observed quasi-reversibility. When we compare these data with the aprotic CV data for all four RMs with **2**, we see a deviation from the trend described for **1** above: the addition of all RMs lead to a completely irreversible wave (**Figure S86**). Notably, TPTD shows a significant increase in current density over DBTD when added to a solution of **2** under CO<sub>2</sub> saturation conditions (**Figure S86B**, red). Variable concentration studies were completed for all systems that produce an electrochemically irreversible system under aprotic conditions: the observed current density is proportional to the concentration of all reaction components (**Figures S87-S103**).

CPE experiments were then performed to assess reaction efficiency under aprotic conditions. Unlike the results for 1+DBTD, all new systems reported here (1 with the new RMs and 2 with all RMs) demonstrated insignificant catalytic properties under tested electrolysis conditions. The CPE experiments for 1 with Mes<sub>2</sub>DBTD and TPTD as the RM and 2 with all four RMs led to a rapid loss of activity: following an initial stable period, current quickly diminishes (Figures S104-S109), with no amount of CO detected above limit of quantification (LOQ, see SI). Initial stability followed by rapid loss of activity suggests molecular adsorption to the electrode, resulting in a passivation of the electrode surface.<sup>43</sup> Comparing these results with control CPE experiments of 1,<sup>19</sup> 2, DBTD,<sup>19</sup> TPTD, Mes<sub>2</sub>DBTD, and Ph<sub>2</sub>DBTD individually under aprotic

conditions (**Figures S110-S113**) also showed either no CO or the presence of non-quantifiable amounts of CO (**Table S41-S43**). A similar phenomenon is observed when Ph<sub>2</sub>DBTD is used as the RM with **1** (**Figure S114**), but in this case the system has a FE<sub>CO</sub> =  $26\pm2\%$  (**Table S44**) and  $^{1}$ H NMR of the post-bulk solution shows the appearance of carbonate (CO<sub>3</sub><sup>2-</sup>), but no other carbon-containing products (**Figure S115**). Although CV data indicates that some of these combinations should result in aprotic catalytic activity, these combinations are not stable under the tested electrolysis conditions.

#### **Discussion:**

Here, both the experimental and computational data indicate that the RM is operating by an inner-sphere mechanism under protic conditions (Figure 8). We propose that first, the fourcoordinate neutral catalyst, i, is reduced to the monoanionic Cr species ii. Based on calculations previously performed on the co-electrocatalytic mechanism of 1,  $CO_2$  readily binds to ii to form [Cr-CO<sub>2</sub>] iii. 8, 18, 19 With PhOH present this species is protonated, binds DMF and is then reduced to form the monoanionic  $[Cr-CO_2H]^-iv$ . The one electron reduced  $[RM]^-$  binds to this species to form v, which we proposed to be the key intermediate,  ${}_{0}^{4}\mathbf{Cr(CO_{2}H)(RM)}^{-2}$ , stabilized by pancake bonding between the one-electron reduced bpy-backbone and the  $\pi$ -framework of the reduced RM. We propose that v is further stabilized when the  $\pi$ -framework of the RM is extended, due to closer energy levels of the orbitals involved in PB and greater dispersive interactions. Furthermore, extended aromatic character can protect the radical character of the RM in the reduced state, aligning with the improved performance of these mediators under electrolysis conditions. Following the addition of a second proton equivalent, the neutral RM is released along with water leaving  $[Cr-CO]^- vi$ , which we have previously shown is not stable.<sup>8</sup> This species then releases CO to form the monoanionic four-coordinate neutral Cr species *ii*, completing the cycle.

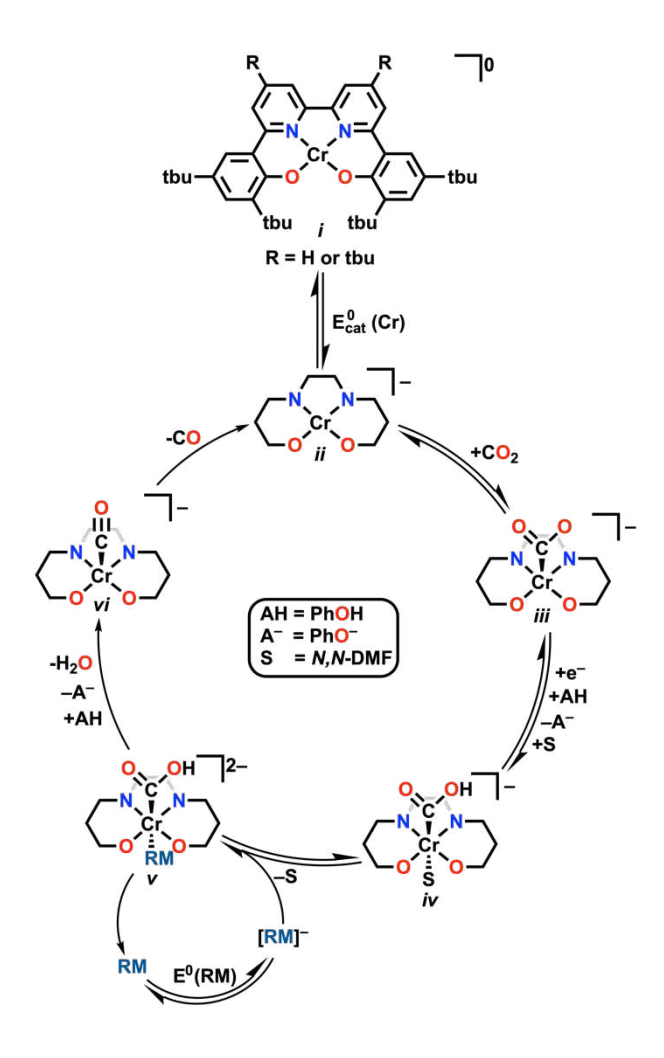


**Figure 8.** Proposed catalytic mechanism for co-electrocatalytic CO<sub>2</sub> reduction by Cr and RM under protic conditions where Cr is 1 or 2 and RM is DBTD, TPTD, Ph<sub>2</sub>DBTD, and Mes<sub>2</sub>DBTD.

Computational results show that the barrier for C–OH bond cleavage in all computed  ${}^4_0\text{Cr}(\text{CO}_2\text{H})(\text{RM})^{-2}$  adducts is roughly equivalent for all possibilities and lower than the corresponding solvento species  ${}^4_0\text{Cr}(\text{CO}_2\text{H})(\text{DMF})^{-1}$ . This means that the equilibrium displacement of the axial solvent ligand by  $[\text{RM}]^-$  dictates whether lower or higher energy catalytic pathways are accessible and will be directly reflected in the rate observed at co-catalytic potentials. Further, the minimal difference in barrier height across the  ${}^4_0\text{Cr}(\text{CO}_2\text{H})(\text{RM})^{-2}$  adducts suggests that minimal changes exist in the bond between sulfone and Cr center, consistent with the proposal

that changes in dispersion effects and PB are responsible for the differences in binding energy. Both TPTD and Ph<sub>2</sub>DBTD show increased activity compared to DBTD and Mes<sub>2</sub>DBTD as RMs when combined with 1 or 2, despite the more negative operating potentials of the latter pair, which is consistent with an inner-sphere process. Although the kinetic complexity of the system precludes straightforward analysis of variable concentration CV data, the proportional increase in current as the catalyst:RM ratio increased observed in CPE suggests that this equilibrium binding interaction is relevant to the catalytic rate expression. This leads to an *inverse scaling effect between RM standard potential and the observed activity*, with greater catalytic activity observed at lower reduction potentials.

Previously, the existence of inverse potential scaling relationships in molecular electrocatalysts for CO<sub>2</sub> reduction has been primarily explained through the kinetic stabilization of key intermediates. Initial work from Savéant and co-workers in 2016 showed that the inclusion of trimethylammonium groups on the catalyst ligand framework resulted in significant kinetic enhancements to CO production under protic conditions at low overpotentials.<sup>6</sup> This kinetic effect at more positive catalyst standard reduction potentials was initially proposed to be the result of Coulombic stabilization of a key [Fe–CO<sub>2</sub>] intermediate, however, a later computational study showed that the relatively long distance (3.8 Å) resulted in effective charge screening by the implicit solvent used.<sup>44</sup> Energy decomposition analysis showed that both through-space and through-structure effects contribute to the stabilization of the [Fe–CO<sub>2</sub>] intermediate, with through-structure being stronger, but both being necessary to kinetic enhancements at low applied potentials. Nichols *et al.* then reported in 2018 that when hydrogen-bond donors are properly positioned in the secondary coordination sphere, significant increases in activity occur with minor variance in the standard reduction potential of the catalyst.<sup>45</sup> Mechanistic experiments again

indicated that this observation resulted from stabilization of the [Fe–CO<sub>2</sub>] intermediate and not the inclusion of acidic amide protons near the catalytic active site. Subsequently, Gotico *et al.* demonstrate that using urea functional groups as multipoint hydrogen-bond donors in similar frameworks could further enhance this kinetic stabilization effect.<sup>46</sup> A recent report from McCrory and co-workers on a non-porphyrinic Co-based catalyst revealed a previously unobserved effect where the combination of ligand reduction potential and electrostatic effects could be manipulated to facilitate the storing of additional charge equivalents, improving catalytic activity for CO<sub>2</sub> reduction at lower catalyst standard potentials.<sup>47</sup>

Our proposed mechanism for inverse potential scaling is unique with respect to these previous examples. Unlike the use of electrostatic effects to stabilize bound CO<sub>2</sub> intermediates or facilitate the storage of electron equivalents in the ligand framework, dispersive interactions and PB drive the association of RM and Cr complex, surmounting the Coulombic repulsion between the two fragments. This co-catalytic assembly presents a lower barrier for the rate-limiting C–OH bond cleavage step. Importantly, this barrier is equivalent across all RMs and instead it is the favorability of the pre-equilibrium comprising the formation of the co-catalytic assembly that dictates the extent the faster mechanism contributes to the observed activity. Mediators with extended aromaticity operate at lower redox potentials, but present stronger PB and dispersive interactions with the metal catalyst, favoring the formation of the co-catalytic assembly and thus yielding enhanced reaction rates at lower overpotential.

#### **Conclusion:**

These results show that by tuning properties of both catalyst and RM, an increase in activity for the co-electrocatalytic reduction of CO<sub>2</sub> can be achieved at lower overpotential by means of inner-sphere electron transfer. Through the addition of electron-donating groups to the bpy

backbone in complex 2, we have improved the activity of our Cr-centered catalyst for CO<sub>2</sub> reduction. Consistent with the proposal in our initial report of co-catalytic systems with 1,<sup>19</sup> these data provide a theoretical and experimental basis for an inner-sphere mechanism under protic conditions. By tuning the stereoelectronic properties of the catalyst and the RM, we have optimized our system to decrease the overpotential while increasing the activity, contrary to what would be predicted by a classical outer-sphere Marcus-theory type model.<sup>32</sup> As a result, an equilibrium solvent displacement reaction can be used to access a lower energy catalytic pathway, with increased favorability driving the system to higher observed activity. Additionally, the selectivity of the parent Cr complexes is retained with all catalytically competent systems being quantitatively selective for CO. Importantly, implementing the strategies identified by this work will be a powerful tool for developing systems which improve the performance of molecular catalyst systems. We are exploring additional strategies to optimize the co-electrocatalytic response in ongoing studies.

#### **Associated Content**

Supporting Information can be found at XXX. SI includes synthetic summaries, NMR and UV-vis characterization, electrochemistry, and description of experimental details and methods, as well as a separate file containing computational coordinates. CCDC 1984949, 1984950, 2150929, 2150930, 2154597, 2154598, and 2154599 contain the crystallographic data for this paper. This data can be accessed free of charge from The Cambridge Crystallographic Data Center via www.ccdc.cam.ac.uk/structures

**Author Contributions.** CWM conceptualized and supervised the project. AGR, JJM, SLH, KRB, IHT, DAD, and CWM designed and conducted experiments. The manuscript was written with analysis and contributions from all authors.

## **Funding Sources**

This research was supported by the U.S. Department of Energy, Office of Science, Office of Basic Energy Sciences, Catalysis Science Program, under Award DE-SC0022219. Single crystal X-ray diffraction experiments were performed on a diffractometer at the University of Virginia funded by the NSF-MRI program (CHE-2018870). We acknowledge UVA for support of the Rivanna High-Performance Computing Center.

#### **References:**

- 1. De Luna, P.; Hahn, C.; Higgins, D.; Jaffer, S. A.; Jaramillo, T. F.; Sargent, E. H. What would it take for renewably powered electrosynthesis to displace petrochemical processes? *Science* **2019**, 364 (6438), eaav3506 DOI: 10.1126/science.aav3506.
- 2. Aresta, M.; Dibenedetto, A.; Angelini, A. Catalysis for the Valorization of Exhaust Carbon: from CO2 to Chemicals, Materials, and Fuels. Technological Use of CO2. *Chem. Rev.* **2014**, 114 (3), 1709-1742 DOI: 10.1021/cr4002758.
- 3. Senftle, T. P.; Carter, E. A. The Holy Grail: Chemistry Enabling an Economically Viable CO2 Capture, Utilization, and Storage Strategy. *Acc. Chem. Res.* **2017**, 50 (3), 472-475 DOI: 10.1021/acs.accounts.6b00479.
- 4. Froehlich, J. D.; Kubiak, C. P. Homogeneous CO2 Reduction by Ni(cyclam) at a Glassy Carbon Electrode. *Iorg. Chem.* **2012**, 51 (7), 3932-3934 DOI: 10.1021/ic3001619.
- 5. Cometto, C.; Chen, L.; Lo, P.-K.; Guo, Z.; Lau, K.-C.; Anxolabéhère-Mallart, E.; Fave, C.; Lau, T.-C.; Robert, M. Highly Selective Molecular Catalysts for the CO2-to-CO Electrochemical Conversion at Very Low Overpotential. Contrasting Fe vs Co Quaterpyridine Complexes upon Mechanistic Studies. *ACS Catal.* **2018**, 8 (4), 3411-3417 DOI: 10.1021/acscatal.7b04412.
- 6. Azcarate, I.; Costentin, C.; Robert, M.; Savéant, J.-M. Through-Space Charge Interaction Substituent Effects in Molecular Catalysis Leading to the Design of the Most Efficient Catalyst of CO2-to-CO Electrochemical Conversion. *J. Am. Chem. Soc.* **2016**, 138 (51), 16639-16644 DOI: 10.1021/jacs.6b07014.
- 7. Sampson, M. D.; Nguyen, A. D.; Grice, K. A.; Moore, C. E.; Rheingold, A. L.; Kubiak, C. P. Manganese Catalysts with Bulky Bipyridine Ligands for the Electrocatalytic Reduction of Carbon Dioxide: Eliminating Dimerization and Altering Catalysis. *J. Am. Chem. Soc.* **2014**, 136 (14), 5460-5471 DOI: 10.1021/ja501252f.
- 8. Hooe, S. L.; Dressel, J. M.; Dickie, D. A.; Machan, C. W. Highly Efficient Electrocatalytic Reduction of CO<sub>2</sub> to CO by a Molecular Chromium Complex. *ACS Catal.* **2020**, 10 (2), 1146-1151 DOI: 10.1021/acscatal.9b04687.
- 9. Babcock, G. T.; Wikström, M. Oxygen activation and the conservation of energy in cell respiration. *Nature* **1992**, 356 (6367), 301-309 DOI: 10.1038/356301a0.
- 10. Anson, C. W.; Ghosh, S.; Hammes-Schiffer, S.; Stahl, S. S. Co(salophen)-Catalyzed Aerobic Oxidation of p-Hydroquinone: Mechanism and Implications for Aerobic Oxidation Catalysis. *J. Am. Chem. Soc.* **2016**, 138 (12), 4186-4193 DOI: 10.1021/jacs.6b00254.

- 11. Anson, C. W.; Stahl, S. S. Cooperative Electrocatalytic O2 Reduction Involving Co(salophen) with p-Hydroquinone as an Electron–Proton Transfer Mediator. *J. Am. Chem. Soc.* **2017**, 139 (51), 18472-18475 DOI: 10.1021/jacs.7b11362.
- 12. Hooe, S. L.; Cook, E. N.; Reid, A. G.; Machan, C. W. Non-covalent assembly of proton donors and p-benzoquinone anions for co-electrocatalytic reduction of dioxygen. *Chem. Sci.* **2021**, 12 (28), 9733-9741 DOI: 10.1039/D1SC01271A.
- 13. Chalkley, M. J.; Del Castillo, T. J.; Matson, B. D.; Peters, J. C. Fe-Mediated Nitrogen Fixation with a Metallocene Mediator: Exploring pKa Effects and Demonstrating Electrocatalysis. *J. Am. Chem. Soc.* **2018**, 140 (19), 6122-6129 DOI: 10.1021/jacs.8b02335.
- 14. McLoughlin, E. A.; Armstrong, K. C.; Waymouth, R. M. Electrochemically Regenerable Hydrogen Atom Acceptors: Mediators in Electrocatalytic Alcohol Oxidation Reactions. *ACS Catal.* **2020**, 10 (19), 11654-11662 DOI: 10.1021/acscatal.0c03240.
- 15. Galvin, C. M.; Waymouth, R. M. Electron-Rich Phenoxyl Mediators Improve Thermodynamic Performance of Electrocatalytic Alcohol Oxidation with an Iridium Pincer Complex. *J. Am. Chem. Soc.* **2020**, 142 (45), 19368-19378 DOI: 10.1021/jacs.0c09605.
- 16. Oh, Y.; Hu, X. L. Organic molecules as mediators and catalysts for photocatalytic and electrocatalytic CO2 reduction. *Chem. Soc. Rev.* **2013**, 42 (6), 2253-2261 DOI: 10.1039/c2cs35276a.
- 17. Smith, P. T.; Weng, S.; Chang, C. J. An NADH-Inspired Redox Mediator Strategy to Promote Second-Sphere Electron and Proton Transfer for Cooperative Electrochemical CO2 Reduction Catalyzed by Iron Porphyrin. *Inorg. Chem.* **2020**, 59 (13), 9270-9278 DOI: 10.1021/acs.inorgchem.0c01162.
- 18. Moreno, J. J.; Hooe, S. L.; Machan, C. W. DFT Study on the Electrocatalytic Reduction of CO<sub>2</sub> to CO by a Molecular Chromium Complex. *Inorg. Chem.* **2021**, 60 (6), 3635-3650 DOI: 10.1021/acs.inorgchem.0c03136.
- 19. (a) Hooe, S. L.; Moreno, J. J.; Reid, A. G.; Cook, E. N.; Machan, C. W. Mediated Inner-Sphere Electron Transfer Induces Homogeneous Reduction of CO<sub>2</sub> via Through-Space Electronic Conjugation\*\*. *Angew. Chem. Int. Ed.* **2022**, 61 (1), e202109645 DOI: <a href="https://doi.org/10.1002/anie.202109645">https://doi.org/10.1002/anie.202109645</a>; (b) *Corrigendum* **2022**, 61, e202205139.
- 20. Li, J. S., Pingchuan; Zhao, Zujin; Tang, Ben Z. Through-Space Conjugation: A Thriving Alternative for Optoelectronic Materials. *CCS Chem.* **2019**, 1 (2), 181-196.
- 21. Garcia-Yoldi, I.; Miller, J. S.; Novoa, J. J. Structure and Stability of the [TCNE]<sub>2</sub><sup>2-</sup> Dimers in Dichloromethane Solution: A Computational Study. *J. Phys. Chem. A.* **2007**, 111 (32), 8020-8027 DOI: 10.1021/jp073188i.
- 22. Garcia-Yoldi, I.; Miller, J. S.; Novoa, J. J. [Cyanil]22– dimers possess long, two-electron ten-center (2e–/10c) multicenter bonding. *Phys. Chem. Chem. Phys.* **2008**, 10 (28), 4106-4109 DOI: 10.1039/B806900J.
- 23. Mota, F.; Miller, J. S.; Novoa, J. J. Comparative Analysis of the Multicenter, Long Bond in [TCNE]— and Phenalenyl Radical Dimers: A Unified Description of Multicenter, Long Bonds. *J. Am. Chem. Soc.* **2009**, 131 (22), 7699-7707 DOI: 10.1021/ja9002298.
- 24. Kertesz, M. Pancake Bonding: An Unusual Pi-Stacking Interaction. *Chem. Eur. J.* **2019**, 25 (2), 400-416 DOI: <a href="https://doi.org/10.1002/chem.201802385">https://doi.org/10.1002/chem.201802385</a>.
- 25. Hooe, S. L.; Rheingold, A. L.; Machan, C. W. Electrocatalytic Reduction of Dioxygen to Hydrogen Peroxide by a Molecular Manganese Complex with a Bipyridine-Containing Schiff Base Ligand. *J. Am. Chem. Soc.* **2018**, 140 (9), 3232-3241 DOI: 10.1021/jacs.7b09027.

- 26. Nichols, A. W.; Chatterjee, S.; Sabat, M.; Machan, C. W. Electrocatalytic Reduction of CO2 to Formate by an Iron Schiff Base Complex. *Inorg. Chem.* **2018**, 57 (4), 2111-2121 DOI: 10.1021/acs.inorgchem.7b02955.
- 27. Hooe, S. L.; Machan, C. W. Dioxygen Reduction to Hydrogen Peroxide by a Molecular Mn Complex: Mechanistic Divergence between Homogeneous and Heterogeneous Reductants. *J. Am. Chem. Soc.* **2019**, 141 (10), 4379-4387 DOI: 10.1021/jacs.8b13373.
- 28. Costentin, C.; Drouet, S.; Robert, M.; Savéant, J.-M. Turnover Numbers, Turnover Frequencies, and Overpotential in Molecular Catalysis of Electrochemical Reactions. Cyclic Voltammetry and Preparative-Scale Electrolysis. *J. Am. Chem. Soc.* **2012**, 134 (27), 11235-11242 DOI: 10.1021/ja303560c.
- 29. Chintala, S. M.; Petroff II, J. T.; Barnes, A.; McCulla, R. D. Photodeoxygenation of phenanthro[4,5-bcd]thiophene S-oxide, triphenyleno[1,12-bcd]thiophene S-oxide and perylo[1,12-bcd]thiophene S-oxide. *J. Sulphur Chem.* **2019**, 40 (5), 503-515 DOI: 10.1080/17415993.2019.1615065.
- 30. Klemm, L. H.; Lawrence, R. F. The insertion and extrusion of heterosulfur bridges. X. Conversions in the triphenylene-triphenylo[4,5-bcd] thiophene system. *J. Heterocycl. Chem.* **1979**, 16 (3), 599-601 DOI: https://doi.org/10.1002/jhet.5570160340.
- 31. Baur, J. E. In *Handbook of Electrochemistry*; Zoski, C. G., Ed.; Elsevier: 2007; pp 829-848.
- 32. Piechota, E. J.; Meyer, G. J. Introduction to Electron Transfer: Theoretical Foundations and Pedagogical Examples. *J. Chem. Educ.* **2019**, 96 (11), 2450-2466 DOI: 10.1021/acs.jchemed.9b00489.
- 33. Elgrishi, N.; McCarthy, B. D.; Rountree, E. S.; Dempsey, J. L. Reaction Pathways of Hydrogen-Evolving Electrocatalysts: Electrochemical and Spectroscopic Studies of Proton-Coupled Electron Transfer Processes. *ACS Catal.* **2016**, 6 (6), 3644-3659 DOI: 10.1021/acscatal.6b00778.
- 34. Frisch, M. J.; Trucks, G. W.; Schlegel, H. B.; Scuseria, G. E.; Robb, M. A.; Cheeseman, J. R.; Scalmani, G.; Barone, V.; Petersson, G. A.; Nakatsuji, H.; Li, X.; Caricato, M.; Marenich, A. V.; Bloino, J.; Janesko, B. G.; Gomperts, R.; Mennucci, B.; Hratchian, H. P.; Ortiz, J. V.; Izmaylov, A. F.; Sonnenberg, J. L.; Williams; Ding, F.; Lipparini, F.; Egidi, F.; Goings, J.; Peng, B.; Petrone, A.; Henderson, T.; Ranasinghe, D.; Zakrzewski, V. G.; Gao, J.; Rega, N.; Zheng, G.; Liang, W.; Hada, M.; Ehara, M.; Toyota, K.; Fukuda, R.; Hasegawa, J.; Ishida, M.; Nakajima, T.; Honda, Y.; Kitao, O.; Nakai, H.; Vreven, T.; Throssell, K.; Montgomery Jr., J. A.; Peralta, J. E.; Ogliaro, F.; Bearpark, M. J.; Heyd, J. J.; Brothers, E. N.; Kudin, K. N.; Staroverov, V. N.; Keith, T. A.; Kobayashi, R.; Normand, J.; Raghavachari, K.; Rendell, A. P.; Burant, J. C.; Iyengar, S. S.; Tomasi, J.; Cossi, M.; Millam, J. M.; Klene, M.; Adamo, C.; Cammi, R.; Ochterski, J. W.; Martin, R. L.; Morokuma, K.; Farkas, O.; Foresman, J. B.; Fox, D. J. Gaussian 16 Rev. B.01, Wallingford, CT, 2016.
- 35. Becke, A. D. Density-functional thermochemistry. III. The role of exact exchange. *J. Chem. Phys.* **1993**, 98 (7), 5648-5652 DOI: doi:http://dx.doi.org/10.1063/1.464913.
- 36. Lee, C.; Yang, W.; Parr, R. G. Development of the Colle-Salvetti correlation-energy formula into a functional of the electron density. *Phys. Rev. B* **1988**, 37 (2), 785-789.
- 37. Vosko, S. H.; Wilk, L.; Nusair, M. Accurate spin-dependent electron liquid correlation energies for local spin density calculations: a critical analysis. *Can. J. Phys.* **1980**, 58 (8), 1200-1211 DOI: 10.1139/p80-159.

- 38. Stephens, P. J.; Devlin, F. J.; Chabalowski, C. F.; Frisch, M. J. Ab Initio Calculation of Vibrational Absorption and Circular Dichroism Spectra Using Density Functional Force Fields. *J. Phys. Chem.* **1994**, 98 (45), 11623-11627 DOI: 10.1021/j100096a001.
- 39. Weigend, F.; Ahlrichs, R. Balanced basis sets of split valence, triple zeta valence and quadruple zeta valence quality for H to Rn: Design and assessment of accuracy. *Phys. Chem. Chem. Phys.* **2005**, 7 (18), 3297-3305 DOI: 10.1039/B508541A.
- 40. Weigend, F. Accurate Coulomb-fitting basis sets for H to Rn. *Phys. Chem. Chem. Phys.* **2006**, 8 (9), 1057-1065 DOI: 10.1039/B515623H.
- 41. Grimme, S.; Antony, J.; Ehrlich, S.; Krieg, H. A consistent and accurate ab initio parametrization of density functional dispersion correction (DFT-D) for the 94 elements H-Pu. J. Chem. Phys. **2010**, 132 (15), 154104 DOI: doi:http://dx.doi.org/10.1063/1.3382344.
- 42. Grimme, S.; Ehrlich, S.; Goerigk, L. Effect of the damping function in dispersion corrected density functional theory. *J. Comput. Chem.* **2011**, 32 (7), 1456-1465 DOI: 10.1002/jcc.21759.
- 43. Lee, K. J.; McCarthy, B. D.; Dempsey, J. L. On decomposition, degradation, and voltammetric deviation: the electrochemist's field guide to identifying precatalyst transformation. *Chem. Soc. Rev.* **2019**, 48 (11), 2927-2945 DOI: 10.1039/C8CS00851E.
- 44. Mao, Y.; Loipersberger, M.; Kron, K. J.; Derrick, J. S.; Chang, C. J.; Sharada, S. M.; Head-Gordon, M. Consistent inclusion of continuum solvation in energy decomposition analysis: theory and application to molecular CO<sub>2</sub> reduction catalysts. *Chem. Sci.* **2021**, 12 (4), 1398-1414 DOI: 10.1039/D0SC05327A.
- 45. Nichols, E. M.; Derrick, J. S.; Nistanaki, S. K.; Smith, P. T.; Chang, C. J. Positional effects of second-sphere amide pendants on electrochemical CO<sub>2</sub> reduction catalyzed by iron porphyrins. *Chem. Sci.* **2018**, 9 (11), 2952-2960 DOI: 10.1039/C7SC04682K.
- 46. Gotico, P.; Boitrel, B.; Guillot, R.; Sircoglou, M.; Quaranta, A.; Halime, Z.; Leibl, W.; Aukauloo, A. Second-Sphere Biomimetic Multipoint Hydrogen-Bonding Patterns to Boost CO<sub>2</sub> Reduction of Iron Porphyrins. *Angew. Chem. Int. Ed.* **2019**, 58 (14), 4504-4509 DOI: <a href="https://doi.org/10.1002/anie.201814339">https://doi.org/10.1002/anie.201814339</a>.
- 47. Nie, W.; Tarnopol, D. E.; McCrory, C. C. L. Enhancing a Molecular Electrocatalyst's Activity for CO2 Reduction by Simultaneously Modulating Three Substituent Effects. *J. Am. Chem. Soc.* **2021**, 143 (10), 3764-3778 DOI: 10.1021/jacs.0c09357.

TOC:

